Computational investigation of the aerodynamic performance of an optimised alternative fuselage shape

Diwan U. Odendaal, Lelanie Smith and Kenneth J. Craig
Department of Mechanical and Aeronautical Engineering, University of Pretoria, Pretoria, South Africa, and
Drewan S. Sanders
Centre for Propulsion and Thermal Power Engineering, Cranfield University, Bedford, UK

Abstract

Purpose – The purpose of this study is to re-evaluation fuselage design when the main wing's has the ability to fulfill stability requirements without the need for a tailplane. The aerodynamic requirements of the fuselage usually involve a trade-off between reducing drag and providing enough length for positioning the empennage to ensure stability. However, if the main wing can fulfill the stability requirements without the need for a tailplane, then the fuselage design requirements can be re-evaluated. The optimisation of the fuselage can then include reducing drag and also providing a component of lift amongst other potential new requirements.

Design/methodology/approach – A careful investigation of parameterisation and trade-off optimisation methods to create such fuselage shapes was performed. The A320 Neo aircraft is optimised using a parameterised 3D fuselage model constructed with a modified PARSEC method and the SHERPA optimisation strategy, which was validated through three case studies. The geometry adjustments in relation to the specific flow phenomena are considered for the three optimal designs to investigate the influencing factors that should be considered for further optimisation.

Findings – The top three aerodynamic designs show a distinctive characteristic in the low aspect ratio thick wing-like aftbody that has pressure drag penalties, and the aftbody camber increased surface area notably improved the fuselage's lift characteristics.

Originality/value – This work contributes to the development of a novel set of design requirements for a fuselage, free from the constraints imposed by stability requirements. By gaining insights into the flow phenomena that influence geometric designs when a lift requirement is introduced to the fuselage, we can understand how the fuselage configuration was optimised. This research lays the groundwork for identifying innovative design criteria that could extend into the integration of propulsion of the aftbody.

Keywords Optimisation, Computational fluid dynamics, Boundary layer ingestrion, Fuselage design

Paper type Research paper

Nomenclature

C_{LV} = Volume-based lift coefficient;
C_{DV} = Volume-based drag coefficient;
C_{DP} = Volume-based pressure drag coefficient;
C_{DF} = Volume-based friction drag coefficient;
D = Drag forceN;
C_P = Pressure coefficient;
L = Lift forceN;
L_F = Fuselage lengthm;
M = Mach number;
R_e = Reynolds number;
U_∞ = Freestream velocitym.s^{-1};
U_x = Streamwise velocity componentm.s^{-1};
Z = Vertical direction for airfoil constructionm; and
X = Streamwise directionm.

The current issue and full text archive of this journal is available on Emerald Insight at: **https://www.emerald.com/insight/1748-8842.htm**

Aircraft Engineering and Aerospace Technology
96/11 (2024) 1–9
Emerald Publishing Limited [ISSN 1748-8842]
[DOI 10.1108/AEAT-11-2023-0297]

Introduction

In reconsidering the conventional tube-and-wing aircraft configuration, there have been multiple suggestions that either radically change the configuration (Liebeck, 2004; Liebeck *et al.*, 1998; Horton and Selinger, 1987; Woolridge, 1983) or optimize based on certain design requirements towards a different configuration (Reist and Zingg, 2017; Drela, 2011; Yutko *et al.*, 2018; Ciliberti *et al.*, 2017). One such configuration, based on the premise that the tailplane becomes unnecessary when static longitudinal stability can be achieved with variations in the main

The authors would like to thank the South African National Research Foundation for its financial support. The authors would also like to thank Christiaan de Wet for his CFD guidance.

Received 6 December 2023
Revised 16 March 2024
Accepted 19 April 2024

wing geometry alone (Agenbag *et al.*, 2009), has been referred to as the wing-body-tail (WBT) configuration (Huyssen *et al.*, 2012; Smith *et al.*, 2017, 2019). Redeveloping the requirements for the fuselage of an aircraft without this requirement leads to a variety of potential new design requirements for the fuselage.

Previous work (Smith *et al.*, 2017) considered low drag bodies, typically shorter, wider bodies, with nose geometries delaying transition and aftbody contours preventing separation (Parsons and Goodson, 1972; Myring, 1972, 1981; Patel and Lee, 1977). If these low-drag bodies are modified to have a defined trailing edge and camber, it is possible to generate lift from the aftbody of the fuselage. This allows flight at a lower lift coefficient (C_L) of the main wing, further reducing the drag of the overall system.

Initial experimental investigations (Huyssen *et al.*, 2012; Davis and Spedding, 2014) indicated that a defined trailing edge can be used to control circulation in the central region of the aircraft. However, there was only indirect support by the findings to support the argument that a defined trailing edge can lead to a reduction in induced drag. Further Reynolds-averaged Navier–Stokes (RANS) simulations conducted by Smith *et al.* (2017) showed that deflection of the aftbody with or without a defined trailing edge leads to an increase in lift, but not without a drag penalty. The suggestion was not to consider discrete section in the geometry but rather to model the fuselage as a continuous unit. Aftbody deflection alone (with no tail) produced net positive lift, effectively adding camber to the previously axisymmetric outline. Though the lift increment was larger when a tail was added, the drag would also increase, and so net benefits in L/D would not necessarily be decisive. It was further noted that such measures were quite sensitive to details of separation over the body and tail, and paradoxically, a preferred arrangement would be to locate a dedicated trailing edge entirely within the bounds of the viscous wake (Agenbag *et al.*, 2009).

The design appeared to offer a reasonable potential as proposed by the wind tunnel tests (Huyssen *et al.*, 2012) and subsequent RANS investigations (Smith *et al.*, 2017, 2019), essentially characterising what could be termed a baseline wing–body–tail configuration with simply specified geometry and no special attention to optimisation of the geometry. Optimisation studies are encumbered by design requirements, modelling fidelity and limitations that often dictate the outcomes. Recently, some authors focus on fuselage optimisation objectives primarily around drag reduction with fuselage construction constraints (windshield angles, cabin shape/volume, aftbody upsweep) (Nicolosi *et al.*, 2016). Some include the increase of lift (Reist and Zingg, 2017), and others also add engine performance (Drela, 2011; Yutko *et al.*, 2018).

This work explores an approach that combines a RANS model with a multi-objective trade-off optimisation model in Star-CCM+, which was validated in Odendaal *et al.* (2023), to optimise fuselages to include lift. Including the geometric suggestions from Huyssen *et al.* (2012) and Smith *et al.* (2017, 2019) towards finding different ideal fuselage shapes. Although the core focus of the work is to investigate the how the underlying flow principles drive the fuselage body optimization to offer potential lift.

Fuselage construction

The baseline simulation consists of the A320 fuselage with the wing attachment pod. The A320 fuselage was designed in SolidWorks by creating a 3D model using 2D diagrams of the A320 Neo. The A320 Neo model is made to scale with a fuselage length of 37.57 m and width of 3.95 m, as given by the Airbus website (Airbus, 2021).

Figure 1 shows parameters defined in a modified version of the PARSEC method (Della Vecchia *et al.*, 2014). The whole fuselage geometry is modelled using 10 surface control points (which was the lowest number of control points that was tested to ensure the geometry does not self-intersect) that connect using two splines. Four pairs of surface control points are controlled by the cross-sectional height parameter (H), where the top surface vertical distance and bottom surface vertical distance are the same distance from the cross-section mid-point. The trailing edge (body-tail) is controlled by the trailing edge deflection angle (α_{TE}) and trailing edge wedge angle (β_{TE}). The trailing edge deflection angle is modified to be able to have an upward and downward tail deflection.

To incorporate optimisation freedom, the cross-section mid-points and surface control points are connected to a rib structure that will control the vertical offset (H) of each cross-section. The amount of cross-section mid-point variation is constrained to a control box shown in Figure 1. Each cross-section horizontal location has a constant offset from each other to minimise construction errors that arise from a spline intersecting with itself. The distance between the cross-sections is governed by the total length of the fuselage, which can be changed.

The leading-edge radius parameter will control the curvature on the nose, but more importantly, make sure that there will be no construction error when any Y (the vertical component of the cross-section of ellipsoid) parameter is vertically shifted up- or downwards.

For the fuselage cross-sectional consideration, a modified cylindrical cross-section geometry is incorporated. The cross-section consists of four surface control points, which are joined by a single spline. The side control points are controlled by a horizontal line (C x Y), which can move below or above the mid-point to create an egg-shaped cross-section. The horizontal line can vary in length to create an oval cross-sectional shape by changing the (C) value.

Parametric constraints

To determine the minimum required height and width for the cabin, the fineness ratio (λ), defined as length/diameter, is evaluated. For comfortable walking and seating in the fuselage aisle, a minimum height of 3.23 m is derived from typical container and pallet dimensions (LD1–LD9) of 1.63 m (Roskam, 1986), combined with average human heights of 1.8 m for males and 1.6 m for females (Raymer, 2012). The resulting cylindrical fuselage cross-section, with a 3.23 m diameter, accommodates four first-class seats (0.72 m width) with a 0.42 m aisle and six economy seats (0.45 m width) with a 0.53 m aisle, totalling a width of 3.23 m. While the A320, with a width of 3.63 m, accommodates six seats across, the minimum cross-section width of 3.23 m is considered acceptable. Determining the minimum fuselage length involves considering the smallest fineness ratio based on the volumetric drag coefficient ($\lambda = 4$) (Torenbeek, 2010). A 3.23 m diameter suggests a fuselage length of 12.92 m, while a suggested fineness ratio of 8 results in a length of 25.84 m. Despite the variance, both lengths fall below the A320 Neo's

Figure 1 Parameterisation of the fuselage in the longitudinal direction and cross-section of the fuselage showcasing a bottom-heavy oval and a top-heavy oval fuselage cross-section

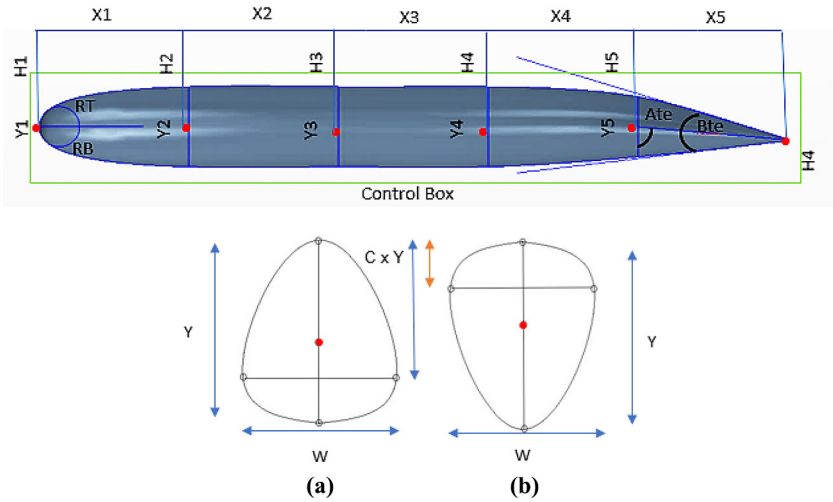

Source: Figure by authors'

fuselage length of 37.57 m (Roskam, 1986). For the tail design, the tail deflection angle (tail upsweep) is crucial to achieve a high angle of attack during take-off, preventing a tail strike. Allowing for a range of 35° deflection upwards and downwards is considered in this investigation. Input ranges for all parameters are detailed in Table 1.

Mesh construction

The mesh construction was similar to the 3D axisymmetric transonic validation study (Odendaal *et al.*, 2023). The domain size for the study indicated a distance of 6 body lengths behind the body was sufficient to capture the drag coefficient with less than one 1% difference. In this work, the inlet surface of the computational domain is located 2 L_f in front of the nose of the fuselage, with a domain height of 4.2 L_f and domain width of 2 L_f. The outlet surface is located 8 L_f away from the trailing edge of the fuselage, as indicated in Figure 2. The computational polyhedral mesh used Advanced Layer Mesher in STAR CCM+ (2013). The function allows for the polyhedral mesh to grow around sharp corners without cells collapsing in on itself. The boundary layer uses 50 prism layers to capture the boundary layer growth along the fuselage.

Table 1 Input parameters for design exploration range

Parameters	Range (m, deg)	Increments (m, deg)	Resolution
Fuselage length	[25, 55]	0.3 m	101
αte	[60, 120]	0.6 deg	101
βte	[10, 60]	0.5 deg	101
C1–C5	[0.25, 0.75]	0.005	101
H1–H5	[7.5, 12.5]	0.05 m	101
LRB and LRT	[0.1, 2]	0.02 m	101
W2–w5	[3.2, 10]	0.14 m	51
W6	[0.1, 10]	0.2 m	51
Y1	[0.1]	0 m	1
Y2–Y4	[3.2, 10]	0.136 m	51
Y5	[2, 5]	0.06 m	51
Y6	[0.05, 5]	0.01 m	51

Source: Table by authors

The volumetric mesh refinement zones follow similar approaches to the 3D axisymmetric transonic validation study completed by Odendaal *et al.* (2023). The first refinement zone is around the fuselage. The inner domain refinement zone size is selected to capture any pressure changes within the domain but also compensate for the change in diameter and width of any optimised fuselage. The wake region is a cone shape extending from the trailing edge to the end of the domain. The wake refinement region has a 35° offset angle to capture the wake as the trailing edge deflection angle is changed by the optimisation algorithm. The grid-convergence index method was used on three different mesh sizes, and mesh convergence was achieved. The mesh consists of 7.21 million cells and is shown in several views in Figure 2.

Boundary conditions, turbulence, transition and optimisation models

The flow was assumed to be steady compressible flow at a Mach number of 0.8. The Reynolds numbers based on the fuselage length were 4.65×10^8, with zero angle of attack and zero side slip. The inlet and side boundary conditions were set to free-stream conditions at atmospheric pressure and temperature at 300 K. The outlet boundary is a pressure boundary set to atmospheric conditions. To save computational time, a symmetry boundary was implemented. The surface of the fuselage has a non-slip wall boundary condition. The non-dimensional wall distance criterion $y^+ < 1$ was satisfied for all optimisation cases.

The Reynolds-average Navier-Stokes (RANS) equation with the shear-stress transport k-w turbulence model (Menter, 1994) was used with the γ-Re_θ transition model. The multi-objective trade-off optimisation algorithm SHERPA was used based on its capability to make large geometrical changes, which constantly refines each parameter input range to provide

Figure 2 A320 Neo domain mesh generation strategy that is also used for the optimisation simulations showing the refinement regions on the fuselage

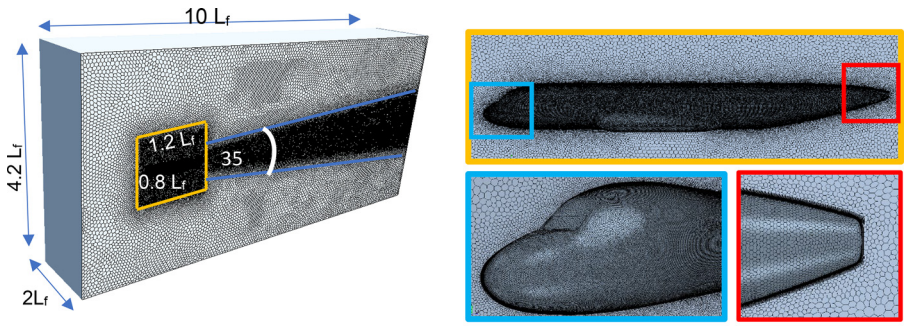

Source: Figure by authors'

multiple optimum geometries. All the models selected were based on the comparative studies and validation completed in Odendaal *et al.* (2023). The simulations were completed on a single personal computer with 16-cores and took approximately 65 days to complete the optimisations.

Geometrical characterization of optimized fuselage shapes

The optimisation simulated 800 designs with the objective of decreasing drag and contributing to lift. Using the fuselage volume as a criterion for an acceptable design, 80% of the designs were regarded as feasible. Seven optimal designs based on lift-to-drag ratio were selected for further investigation. An input parameter sensitivity analysis for the seven optimal designs, based on mean and standard deviation (σ) values, was conducted to investigate the effects of fuselage geometry variation. Note that the vertical height factor (C) and width (W) can be seen as the vertical location of the fuselages' "wing-like" geometry. The results of this sensitivity study can be summarised as follows:

- The trailing edge deflection angle (αte) determines the overall camber of the aftbody of the fuselage; the mean value was 81.15° with a σ of 1.72°. Therefore, this indicates an overall downward camber;
- The trailing edge wedge angle βte controls the slenderness of the aftbody of the fuselage. The mean value of 27° with a σ of 9.57° indicates the fuselage has a thick aftbody;
- The top and bottom leading-edge radius (LRB and LRT) have mean values of 0.95 m and 1.278 m, respectively, with a σ of 0.036 m and 0.032 m. This indicates lager upper nose radius;
- The vertical control point offset (H) has a starting distance of 10 m and can shift a body section higher (H < 10 m) or lower (H > 10 m). The shape of fuselages from the nose to 4/5 of the fuselage length, the centre-points moves slightly upwards. The aft-portion (last 1/5) of the fuselage is cambered downwards;
- The fuselage vertical height (Y) controls the height of each cross-section. Y1 was kept constant at 0.1 m to ensure that the fuselage lofting procedure works for any given input

Figure 3 Designs 3–5 fuselage geometry comparison using its constructed parameters

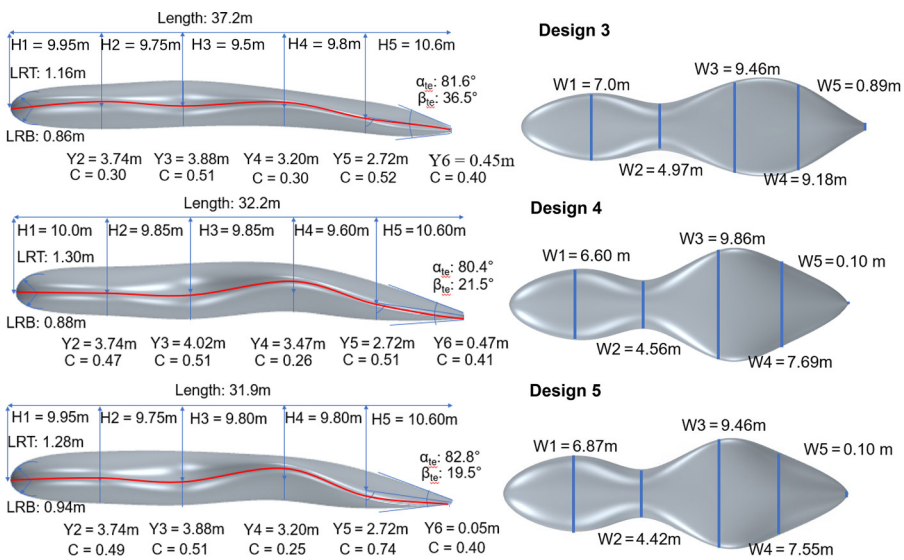

Source: Figure by authors'

parameter. Looking at the mean value trend, the fuselage follows a teardrop shape, with a large maximum height located at the head-to-neck section of the fuselage, followed by a tapered aft-body; and

- The mean width (W2–W6) trend is a widening at the head of the fuselage followed by a narrow neck section. After the neck section, the fuselage body widens substantially and tapers off to the trailing edge.

Overall, statistical analysis of 640 feasible fuselages reveals a general trend in mean fuselage geometry resulting from trade-off optimisation, although each fuselage maintains a unique shape. The overall volume was fixed to be similar to the A320 Neo, and useful volume was maintained between *Y2* and *Y5*, as indicated in Table 1. A comparison of the top 3 L/D geometries illustrates differences in top and side views, emphasising the impact of optimisation on distinct fuselage shapes (Designs 3, 4 and 5). Figure 3 provides a visual representation of parameter values and vertical height factor lines for each fuselage.

Aerodynamic effect of geometric characteristics of optimised fuselages

Table 2 shows a summary of volume-based drag C_{Dv} and lift coefficient C_{Lv} for fuselage Designs 3–5 and A320 Neo. As expected, C_{Lv} of Designs 3–5 has drastically increased for all optimised fuselages compared to the A320 Neo, which was not designed to consider lift contribution. As a consequence of the lift contribution that was not constrained, C_{Dv} also increased due to an increase in pressure (C_{DP}) and friction (C_{DF}) drag components. Considering the individual drag components, for all the optimised cases as well as the A320 Neo, the pressure drag component is 75% of C_{Dv} for the fuselage, allowing commentary on the trends of the fuselage shape rather than the absolute values of C_{Dv}. Although this is not an ideal solution for designing the fuselage, the trends observed in terms of shape modification towards producing a component of lift were of interest, and the following section will consider the details of the fluid dynamics underlying the geometric trends.

Table 2 Summary of lift and drag volumetric coefficients for fuselage Designs 3–5 and A320 Neo which is the comparative baseline

Fuselage	CDv	CDP	CDF	CLv	L/D	L/D increase (%)
Design 3	0.0465	0.0348	0.0116	0.2398	5.156	1,164
Design 4	0.0665	0.0498	0.0166	0.3363	5.052	1,138
Design 5	0.0841	0.0631	0.0210	0.4131	4.906	1,103
A320 Neo	0.0173	0.0129	0.0043	0.0071	0.408	–

Source: Table by authors

Boundary layer separation effects

To clarify the smaller 25% contribution experienced from C_{DF}, the relative streamwise velocity is considered. Figure 4 shows the U_x/U_∞ contours using a cell surface with zoomed-in images of the trailing edges of the aftbodies. The U_x/U_∞ contours maximum magnitude was set to 0 with normal free-ranging minimum magnitude to show where possible boundary layer separation occurs. Design 3 experiences a small area of flow recirculation, mainly on the centre aftbody in the tail section. Design 5 has a long, slender area of recirculation also at the centre aftbody in the tail section.

Figure 5(a) and (b), shows the streamwise velocity vectors and transverse velocity vectors with refinement near the surface for Designs 3 to 5. The streamwise velocity vectors are captured at the point of separation until the trailing edge but two locations are used for Design 5 due to the large separation area. The transverse velocity vectors are captured at $X/L_f = 1.05$ indicated by the red line. Design 4 streamwise velocity vector shows that there is a small portion of reverse flow at the trailing edge where the upwards and streamwise flow meet. Design 3 streamwise velocity vector shows that there is flow separation and attachment near the trailing edge, which indicates that there is a flow separation bubble. This happens due to an upwash that wraps around the top surface trailing edge, forcing slow-moving air in the flow separation region to flow down and backward. Design 5's upwash is not as developed as that of Design 3, which causes a dispersed upwards flow pattern. The flow separation region remains detached at the centreline.

Looking at Figure 5(b), there are two vortex cores present for all fuselage designs. There is a counter clockwise vortex that forms after the widest portion of the fuselage and a clockwise vortex at the trailing edge of the fuselage. There is upwash at the aft portion of the fuselage due to the fuselage geometry becoming more perpendicular to the freestream direction. This phenomenon forces slow-moving air near the centre trailing

Figure 4 Streamwise relative velocity (Ux/U∞) contour plots on Designs 3–5 to showcase skin friction component

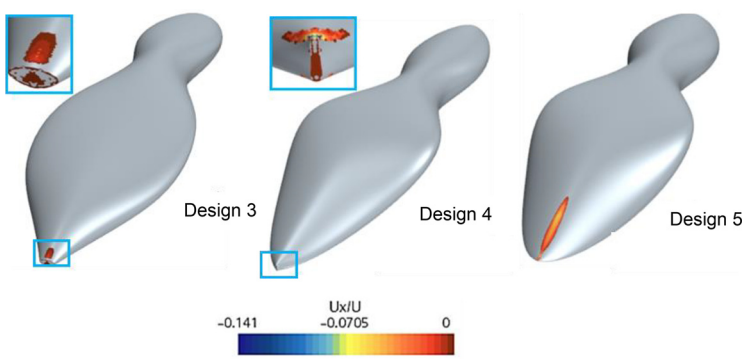

Source: Figure by authors'

Figure 5 Streamwise velocity vector glyphs for Designs 3–5 are shown on the left-hand side. Transverse velocity vector glyphs for Designs 3–5 are shown on the right-hand side which correlates with the red line location on the left-hand side. The blue box is an enlargement of the vortex at the centreline of the fuselage

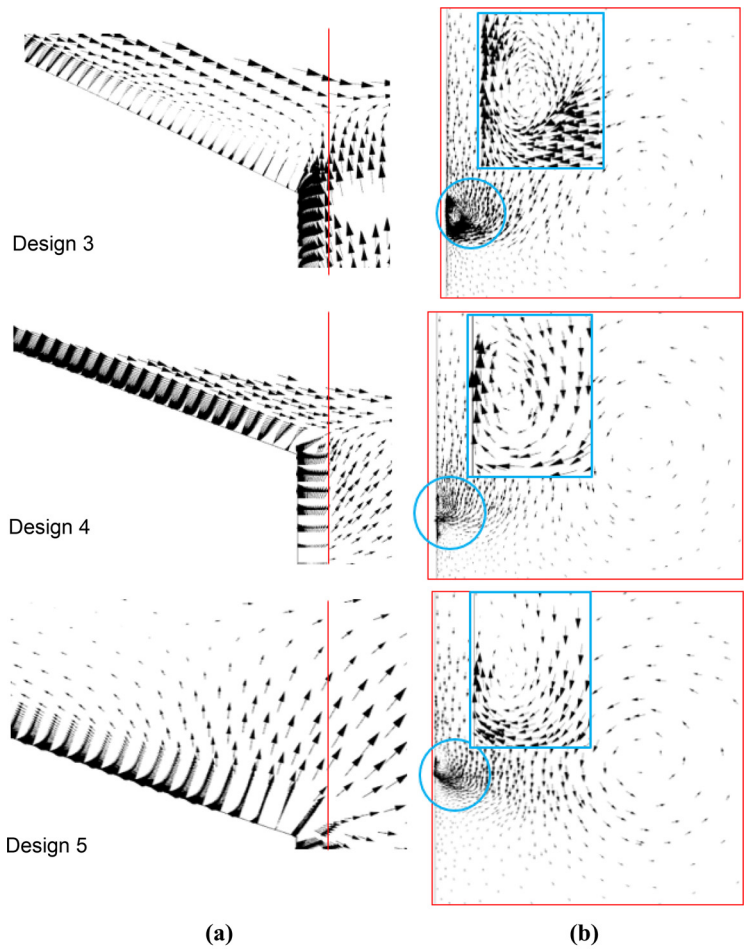

Source: Figure by authors'

edge to move towards the centre, which is then influenced by strong upwash, creating the clockwise vortex.

Wake analysis

Figure 6 shows the area of U_x/U_∞ at a plane location $X/L_f = 1.01$, and the bottom shows the U_x/U_∞ at the horizontal centre-point of the trailing-edge for each fuselage. The A320 Neo has the largest wake thickness due to the upswept tail that increases boundary layer thickness on the bottom surface. The fluid patterns around the three optimal designs are investigated to gain perspective on the mechanisms that lead to the flow features we observe around the wake profile.

In general, the slowest moving air is at the centre trailing edge, as it is the closest to the plane, but for the outside regions, the plume of slow-moving air steadily returns to free stream velocity as the distance between the fuselage and the plane increases. The more rounded aftbody of Design 3 has a large, almost uniform, slow-moving air plume. Alternatively, Designs 4 and 5 feature a continuously tapered aftbody, which leads to a smaller volume of slow-moving air.

Due to the upsweep tail geometry of the A320 Neo, there is a substantial volume of relative velocity that is vertically oriented. Generally, Designs 3–5 exhibit a main vortex offset to the left, but it is evident that the main vortex in Design 3 is weaker than that of Designs 4 and 5.

Compressibility effects

An iso-surface (set to Mach = 1) contouring part is used to visualise the boundary where flow has Mach > 1 in a 3D domain. The top and side views of the iso-surface Mach number contouring for Designs 3–5 are shown in Figure 7.

Designs 3–5 have two areas where flow exceeds Mach = 1 (referred to as major and minor supersonic area) that form at the 2nd fuselage widening section in the midbody region. The major supersonic area starts at the top surface of the fuselage, wraps around the widest part of the fuselage and ends on the bottom surface. The second, smaller supersonic area is located on the top surface of the fuselage, just after the termination area of the first supersonic area. Design 3 has the smallest volume of major and minor supersonic area, while Design 4 has the largest volume for the major supersonic area, maintaining the same

Figure 6 3D volume relative velocity Ux/U∞ contouring on front and side view for fuselage Designs 3–5 and A320 Neo

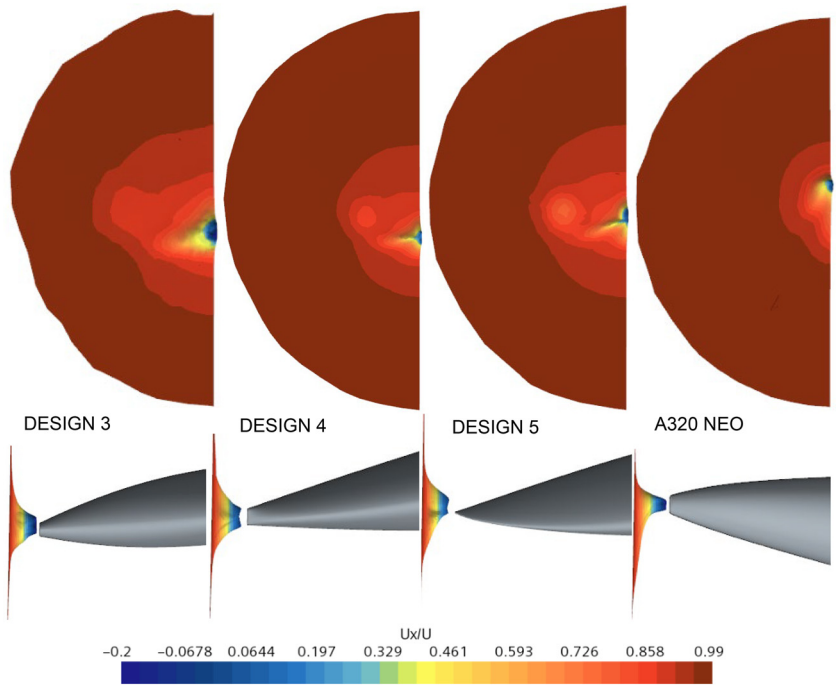

Source: Figure by authors'

Figure 7 The boundary where flow has Mach > 1 in a 3D domain on the optimised Designs 3–5

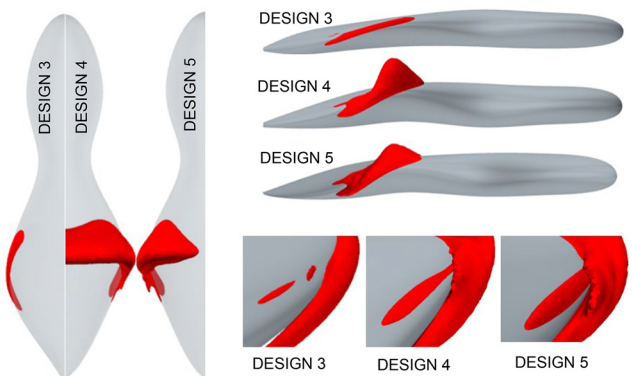

Source: Figure by authors'

supersonic area height over the entire top surface. The minor supersonic area is more developed in comparison to Design 3. Design 5 has major supersonic area with a smaller height and volume than Design 4. The highest point of the major supersonic area is directly above the widest edge of the fuselage and terminates before the fuselage's longitudinal centreline. This outer portion angle of attack causes the free stream velocity to significantly increase over and around the top surface, reaching supersonic flow conditions of Mach 1.

At the centreline of Designs 3 and 5, the fuselage has a flat top surface, from the nose to the apex point of the fuselage body chamber. This allows air velocity to accelerate over the fuselage but does not reach critical Mach values, whereas Design 4 has a fuselage chamber apex point higher than the nose region which increased the air velocity to reach supersonic flow conditions. Ideally, shockwaves would want to be avoided, and any transition to supersonic flow could lead to a shock forming, which should be carefully considered if integrated propulsion is required on the aftbody.

Lift potential

Figure 8 shows the pressure distributions of the three optimised fuselages at the centre of the fuselage (0 m) and at an offset of 2 m. In general, there are mainly two regions that generate downforce (red arrow) and two regions that generate lift (blue arrow). The offset pressure distributions show a larger differential between the top and bottom surfaces. This is an indication that most of the lifting capacity is due to the low area ratio (AR) wing-

Figure 8 Pressure coefficient distribution at 0 and 2 m offset for Designs 3–5

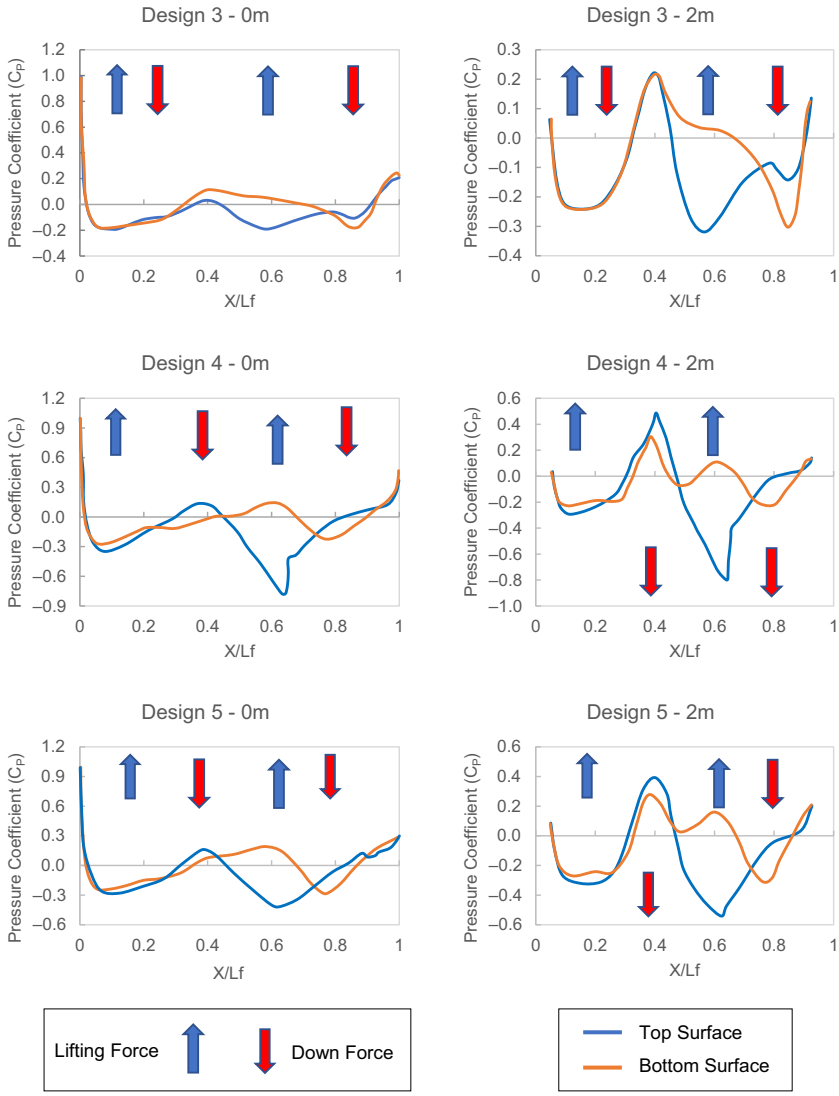

Source: Figure by authors'

like aftbody that the optimised fuselage geometries have. It also appears that Designs 4 and 5 have a narrower spread of the aftbody compared to Design 3, which leads to larger lift components. Designs 4 and 5 have an indentation (between $X/L_f = 0.5$ to 0.7) on the bottom surface at the midbody section, which increases pressure, resulting in a larger C_p differential which increases total lift production at the aftbody. Conversely, Design 3 has an oval-shaped midbody, which increases total surface area and, therefore, increases the total lift produced, compared with Designs 4 and 5, which have a tapered flat midbody section that becomes a low AR wing.

Conclusion

A multi-objective trade-off study using a modified PARSEC method is applied to a conceptual fuselage design for an alternative WBT configuration. The goal was to reduce drag while also contributing to an unconstrained component of lift. Out of 640 feasible optimised fuselages, the top three performers (based on L/D) were selected for analysis to consider the geometric features developed for these designs and their impact on fluid dynamics. The optimised fuselage designs included a front section that was somewhat flattened and led into a narrower neck section with an aftbody section that was cambered with a flat-diamond shape.

A high-pressure region exists on the bottom side of the fuselage due to the cambered aft portion of the fuselage. The difference in pressure causes lift, and the optimised fuselage enhances the fuselage's lifting ability by having a wide diamond shape aftbody to increase total surface area as well as allowing for a low AR wing-like shape to form two distinct vortex cores. Furthermore, at the edge of the widening section, the fuselage body has an increased angle of incidence (washout), which increases the ability to generate lift. These distinct vortex cores also open up the potential for harnessing the energy deposited into the wake through boundary layer ingestion devices.

While the current approach proves valuable with parameter sweeps for idealised fuselage bodies, its expansion is necessary to model realistic operating conditions, incorporating pitch stability and control as initial design constraints. This expanded approach could provide deeper insights into the complex dynamics of the system. However, in a systematic attempt to develop this approach, this study represents an initial step in modelling and optimising a fuselage in isolation, catering to unique requirements. As part of a broader effort to establish new design requirements, the investigation will extend beyond L/D, exploring energy-based approaches such as the power balance method (Drela, 2011).

References

Agenbag, D.S., Theron, N.J. and Huyssen, R.J. (2009), "Pitch handling qualities investigation of the tailless gull wing configuration", *Journal of Aircraft*, Vol. 46 No. 2, pp. 683-691, doi: 10.2514/1.39755.

Airbus (2021), "Airbus A320neo", Airbus:, available at: www.airbus.com/aircraft/passenger-aircraft/a320-family/a320neo.html

Ciliberti, D., Della Vecchia, P., Nicolosi, F. and De Marco, A. (2017), "Aircraft directional stability and vertical tail design: a review of semi-empirical methods", *Progress in Aerospace Sciences*, Vol. 95, pp. 140-172.

Davis, T.W. and Spedding, G.R. (2014), "Lift and drag measurements of a gull-wing configuration aircraft", 53rd AIAA Aerospace Sciences Meeting, AIAA Paper 2014-0027.

Della Vecchia, P., Daniele, E. and D'Amato, E. (2014), "An airfoil shape optimisation technique coupling PARSEC parameterisation and evolutionary algorithm", *Aerospace Science and Technology*, Vol. 32 No. 1, pp. 103-110.

Drela, M. (2011), "Development of the D8 transport configuration", *29th AIAA Applied Aerodynamics Conference, AIAA 2011-3970, Honolulu, HI*, pp. 27-30.

Horton, R. and Selinger, P.F. (1987), *Nurflügel: Die Geschichte der Horten-Fluzeuge 1933–1960*, Weishaupt Verlag, Graz.

Huyssen, R.J., Spedding, G.R., Mathews, E.H. and Liebenberg, L. (2012), "Wing–body circulation control by means of a fuselage trailing edge", *Journal of Aircraft*, Vol. 49 No. 5, pp. 1279-1289.

Liebeck, R.H. (2004), "Design of the blended wing body subsonic transport", *Journal of Aircraft*, Vol. 41 No. 1, pp. 10-25.

Liebeck, R.H., Page, M.A. and Rawdon, B.K. (1998), "Blended-Wing–body subsonic commercial transport", 36th AIAA Aerospace Sciences Meeting and Exhibit, AIAA Paper 1998-0438, doi: 10.2514/6.1998-438

Menter, F.R. (1994), "Two-equation eddy-viscosity turbulence models for engineering applications", *AIAA Journal*, Vol. 32 No. 8, pp. 1598-1605, doi: 10.2514/3.12149, doi

Myring, D.F. (1981),"A theoretical study of the effects of body shape and Mach number on the drag bodies of revolution in subcritical axisymmetric flow", *Royal Aircraft Establishment TR 8100*, Farnborough, Hants.

Myring, D.F. (1972),"The profile drag of bodies of revolution in subsonic axisymmetric flow", *Royal Aircraft Establishment TR 72234*, Farnborough, Hants.

Nicolosi, F., Della Vecchia, P., Ciliberti, D. and Cusati, V. (2016), "Fuselage aerodynamic prediction methods", *Aerospace Science and Technology*, Vol. 55, pp. 332-343.

Odendaal, D.U., Craig, K.J., Smith, L., Mutungara, N.E. and Sanders, D.S. (2023), "Validation of an approach towards fuselage optimization for effective boundary layer ingestion", AIAA 2023-1555. AIAA SCITECH 2023 Forum.

Parsons, J.S. and Goodson, R.E. (1972), "Optimum shaping of axisymmetric bodies for minimum drag in incompressible flow", Ph.D. Dissertation, Purdue Univ., West Lafayette, IN.

Patel, V.C. and Lee, Y.T. (1977),*Thick Axisymmetric Turbulent Boundary Layer and near Wake of a Low-Drag Body of Revolution*, IA Inst. of Hydraulic Research, Univ. of IA Rept. 210, IA City, IA.

Raymer, D. (2012), *Aircraft Design: A Conceptual Approach*, American Institute of Aeronautics and Astronautics.

Reist, T.A. and Zingg, D. (2017), "High-fidelity aerodynamic shape optimisation of a lifting-fuselage concept for regional aircraft", *Journal of Aircraft*, Vol. 54 No. 3, pp. 1085-1097.

Roskam, J. (1986), *Airplane Design Part III: Layout Design of Cockpit, Fuselage, Wing and Empennage: Cutaways and Inboard Profiles*, DAR, Lawrence, Kan.

Smith, L., Craig, K.J., Meyer, J.P. and Spedding, G.R. (2017), "Modifying low-drag bodies to generate lift: a computational study", *Journal of Aircraft*, Vol. 54 No. 3, pp. 1150-1161.

Smith, L., Craig, K.J., Meyer, J.P. and Spedding, G.R. (2019), "Numerical investigation of the aerodynamic performance for an alternative wing–body–tail configuration", *Journal of Aircraft*, Vol. 56 No. 1, pp. 250-261.

STAR CCM+ (2013), *Star-CCM_ User's Guide, Version 8.06*, CD-Adapco, Melville, New York, NY.

Torenbeek, E. (2010), *Synthesis of Subsonic Airplane Design: An Introduction to the Preliminary Design of Subsonic General Aviation and Transport Aircraft, with Emphasis on Layout, Aerodynamic Design, Propulsion and Performance*, Springer Science & Business Media, Dordrecht.

Woolridge, E. (1983), *Winged Wonders: The Story of the Flying Wings*, Smithsonian Inst. Press.

Yutko, B., Titchener, N., Courtin, C., Lieu, M., Wirsing, L., Hall, D., Tylko, J., Chambers, J., Roberts, T. and Church, C. (2018), "Design and development of the D8 commercial transport concept", 31st Congress of the International Council of the Aeronautical Sciences, *ICAS-2018-D8, Belo Horzonte, Brazil*.

Corresponding author

Diwan U. Odendaal can be contacted at: diwanodendaal@gmail.com